NON-DESTRUCTIVE BEAM PROFILE MONITORS*

C.P. Welsch†, University of Liverpool and Cockcroft Institute, UK

Abstract

This paper presents an overview and comparison between beam induced fluorescence, residual gas ionization and gas jet based beam profile monitors, based on recent experimental and theoretical results at different labs. The achievable image/profile quality and resolution limits will be discussed, along with design consideration for different particle species and primary beam energies. Details are also provided about different classic and novel approaches to gas jet shaping, including nozzle-skimmer and Freznel Zone Plate configurations. Finally, particular challenges such as those arising from monitoring multiple beams in parallel (e.g. proton and electron beam in HLLHC) and solutions for targeting the energy limit within the HLLHC project will be presented.

INTRODUCTION

Non-destructive or minimally-invasive beam profile monitors which can operate in real time are desirable for any particle accelerator. They become a requirement in highest energy/highest intensity machines where many of the commonly used beam monitors will simply no longer work. Some of the possible hosts for such a device are the Large Hadron Collider (LHC) at CERN and its future upgrades, and the high power linac at the European Spallation Source (ESS) [1] where the power of the beam does not allow conventional diagnostics to operate. For some low energy storage rings such as the Ultra-low energy Storage Ring (USR) [2] and the Extra Low Energy Antiproton ring (ELENA) [3], it would also be desirable to have a new breed of diagnostics to avoid deterioration of the particle beam and preserve the vacuum.

GAS-BASED IMAGING TECHNIQUES

Non-invasive gas-based beam profile monitors include residual gas ionization profile monitors (IPM) [4]-[8] and beam induced fluorescence monitors (BIF) [6], [9]-[11]. Both will be briefly presented in the following sections.

Ionization Profile Monitors (IPMs)

IPMs operate by using an external electric field to collect the ions or electrons produced by the interaction of the projectile beam with the residual gas in the vacuum chamber. When IPMs are used to measure the beam profile of low current beams, ion detection is preferred rather than electron detection because the generated ions will have a much lower transverse velocity spread than the generated electrons, due to their mass difference. The image broadening from the transverse thermal spread can be minimized by applying a higher extraction voltage to reduce the collection time. However, for high beam intensity, the space charge field from the projectile beam is comparable to the IPM extraction electric field. In this situation, electron detection is used with an additional parallel dipole magnetic field. The field is used to guide the electrons, which spiral around the magnetic field lines until they reach the detector; in this way it mitigates the influence of the space charge of the projectile beam.

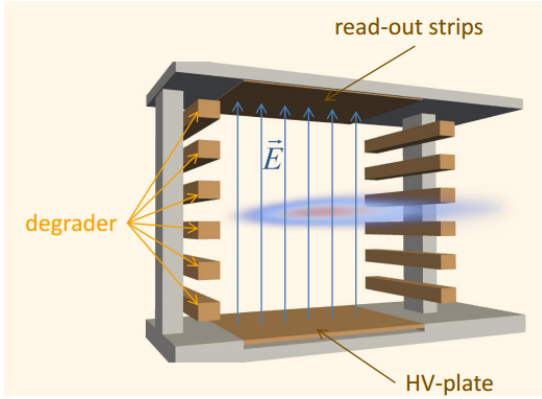

Figure 1: Schematic drawing of the IPM functioning principle. Image courtesy of GSI.

To obtain beam profiles in both transverse planes, two IPM's oriented at right angles have been suggested [9], but the two beam profiles are not acquired at exactly the same location. Nevertheless, in a very low pressure environment, such a device is limited in both acquisition speed and resolution due to signal reduction.

Beam Induced Fluorescence Monitors (BIFs)

BIF monitors rely, like Ionization Profile Monitors (IPMs), on the interaction of beam ions with any working gas, residual or specifically introduced. The differential energy loss of beam ions is the driver for ionization and excitation of the working gas and the beam itself. As long as one can assume that the location of the exciting beam ions and the emitting gas particles are nearly identical, fluorescence light can be used to image the beam particle distribution. A sensitive, spatially resolving photo detection system can then be used for fluorescence imaging, e.g. intensified cameras or PMT-arrays as shown in Fig. 2. For BIF monitors, not only is the cross-section significantly lower as compared to IPMs, but also the induced photons are emitted at all angles and are detected by the camera into a solid angle of only about 10^{-4} . This results in a much lower signal than that of an IPM equipped with a Micro Channel Plate detector (MCP) and an amplification of five to six orders of magnitude. Therefore, a local pressure bump about 10^{-5} mbar is normally required in the detection region even with an intensified CCD or a modern electron-multiplying CCD [10]. This limits its application in an ultra-high vacuum environment.

* Work supported by the EU under grants 215080, 289191 and 721559, the HLLHC-UK project and the STFC CI core grant.
† c.p.welsch@liverpool.ac.uk

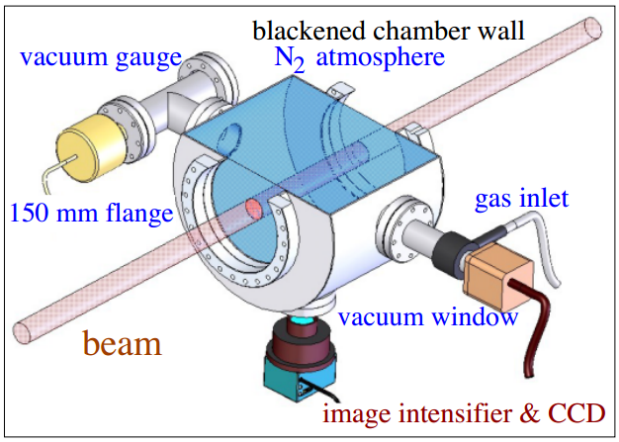

Figure 2: Schematic drawing of the BIF functioning principle. Image courtesy of GSI.

Gas Jet-based Techniques

A feasible solution to overcome these limitations is to use a cold (<20 K) supersonic gas jet shaped into a thin curtain which allows for 2-dimensional beam profile imaging [12] in the same way as an interceptive screen. Such a monitor could be seen as an enhanced IPM where additional gas injection improves the reaction rate and resolution, and reduces the acquisition time, even in an ultra-high vacuum environment. Furthermore, it allows for a simultaneous determination of both transverse beam profiles in a single shot measurement by integration along the X or Y axis. Fig. 3 illustrates the 2-dimensional imaging principle.

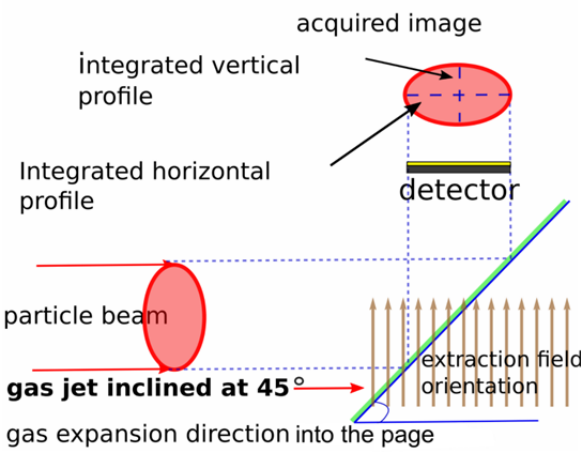

Figure 3: Principle of 2-dimensional imaging (Ions are extracted by the external electric field).

The use of gas jets in beam profile monitoring can be traced back more than four decades, when metal vapor [13], [14] and carbon vapor [15] were used. Recently, it was applied in the Heavy Ion Medical Accelerator (HIMAC) [16] in Chiba, Japan, where an oxygen gas jet was used. This monitor [17] is skimmed and shaped to a thin curtain by focusing magnets [18] to measure the 2D profile of carbon ion beams. Another application by the same author was at the Japan Proton Accelerator Research Complex (J-PARC) [19]. With a molecular nitrogen jet it was possible to measure the proton beam bi-dimensional profile [20]. For both cases, the compression gauge or through gauge method was used to identify the 2-D density distributions of the jets, which showed the thinness and homogeneity of the jet density distribution [17], [21]. Another earlier example is a proton polarimeter with polarized atomic hydrogen jet, used as an independent beam profile monitor by Tsang et al. for the Relativistic Heavy Ion Collider (RHIC) at Brookhaven National Laboratory [22]. It uses the fluorescent light emitted by the excited hydrogen atoms from the interaction between the projectile proton beam and the hydrogen jet. As this monitor is not designed for the purpose, the beam profile measurement is limited to the vertical plane of the accelerator. Compared to residual gas monitoring IPMs or fluorescence monitors, the supersonic gas jet based beam profile monitor offers several advantages. Firstly, the monitor is intrinsically very flexible, in that the interaction it relies upon, namely ionization or fluorescence, is well understood and applicable to most projectile species. Secondly, operating parameters such as acquisition rate and beam perturbation can be easily scaled by varying the target gas density, and tailored for the particular application. The gas jet based beam profile monitor can therefore be used in most accelerators across large energy, current and vacuum ranges, and is not restricted only to low energy storage rings such as the USR, which is the target environment of our supersonic gas jet monitor. In the USR a low intensity antiproton beam with a short life time travels in an ultra-high vacuum.

The basic components of the supersonic gas jet beam profile monitor closely match those needed for a Reaction Microscope (ReMi) which is a momentum spectroscope for analysis of fragmentation molecular and atomic reactions, as for example developed at the Max Planck institute for Nuclear Physics in Heidelberg [23]. Currently, the supersonic gas jet monitor shares the design of components with the ReMi including the Position Sensitive Detector (PSD) for the imaging of ions, the electric field based extraction system and the supersonic gas jet target. Previously, it had also been proposed to operate the ReMi as a transverse beam profile monitor at the point of interaction [24]. The following sections will focus on the basic principles and current state-of-the-art in gas jet based monitors, further details can be found in [25].

GAS JET: OPERATING PRINCIPLE

The operating principle of the gas jet beam profile monitor is as follows: At the particle beam-gas intersection point, ionization occurs and gas ions are created inside the collision volume. These ions are then extracted by an electric field of tunable strength provided by the extraction electrodes, and accelerated towards a position-sensitive detector composed of an MCP and a phosphor screen. The MCP can provide amplification of up to 10^6 without disturbing the position information on the phos-

ISBN 978-3-95450-182-3

phor screen. For every ion that enters the channels of the MCP a shower of electrons is produced, which impacts on the phosphor screen. As a result, visible light is produced and recorded by a camera located behind a transparent viewport outside the vacuum chamber.

In the following, this paper gives a brief description of the jet design and its main properties, ionization rates and details about the monitor resolution. Results from first operational experience with the pulsed valve and two different thicknesses of gas jet curtains, as used in an ultra-high vacuum system to detect a low energy (~3.5 keV, ~7 μA) electron beam are also given.

A general description of the experimental setup is presented in Fig. 4. The gas is stored in a pressurized tank and released into the system with an initial pressure of 1-10 bars. As it travels downstream it passes through a 30 μm diameter circular nozzle which is laser-drilled in a 300 μm thick platinum foil. At this stage, due to the high-pressure differential of about 10^6, most of the collisions between the gas molecules occur in the high-density region near the nozzle. The gas molecules are accelerated by these collisions and undergo free expansion after the nozzle, resulting to the formation of a jet with a very cold inner core stretching a few cm downstream from the nozzle [26].

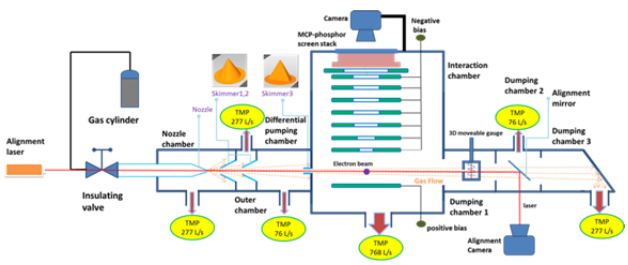

Figure 4: Principle of 2-dimensional imaging (Ions are extracted by a moderate electric field orthogonal to the direction of travel of the gas jet).

Beyond that point, the number of collisions decreases dramatically, until only a few collisions take place and the flow is said to be molecular, before any shock occurs. Given the nozzle size of 30 μm, the point beyond which no more collisions are expected to occur is a few mm from the nozzle. This is negligible compared to the distance to the interaction point, which is 583 mm.

To limit gas usage and control gas flow, as well as to conserve better vacuum conditions, a MHE3-MS1H-3/2G-1/8 solenoid pulsed valve by Festo [27] is used. It features a maximum switching frequency of 280 Hz with 2 ms switching time, an operating pressure from 0 to 8 bar and a standard nominal flow rate of 200 l/min. A TGP110 pulse generator manufactured by Aim & Thurlby Thandar Instruments [28] is used to trigger the pulsed valve externally. It offers a frequency range variable from 0.1 Hz to 10 MHz and an individually-adjustable pulsed width and pulse delay. Its maximum output amplitude is 10 V, which is less than the required valve operating voltage of 24 V. A DC power supply IPS-3303 manufactured by ISO-Tech [29] and a solid state relay DMO063 manufactured by Crydom [30] are used to drive the valve.

This jet is then further shaped by several skimmers. These separate several differentially pumped vacuum chambers through which the jet passes until it reaches a final "reaction chamber", held at a pressure of 10^{-9}-10^{-12} mbar [31, 32]. When entering this chamber the jet has already been shaped by a final rectangular skimmer into a curtain that crosses the primary beam to be analyzed under an angle of 45°. In this interaction, impact ionization of the jet particles occurs and the resulting ions are imaged by a moderate electric field of some kV/m onto a position-sensitive double layer Micro Channel Plate (MCP) detector. The MCP provides signal amplification of up to 10^6. Finally, the resulting beam profile is observed by a Phosphor screen-camera combination that is mounted on the top of the reaction chamber, see Fig. 4.

Proof-of-principle measurements were completed at the Cockcroft Institute [25, 31]. An example profile obtained by crossing the gas jet with a 5 keV electron beam is shown in Fig. 5. It shows the profile of the electron beam as measured with the gas jet, as well as a signal obtained from ionization of the residual gas.

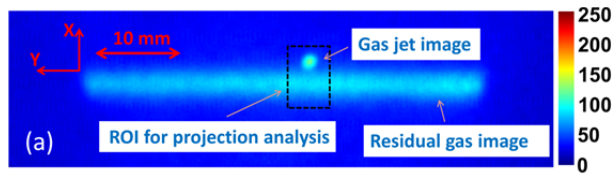

Figure 5: Beam profile of a 5 keV electron beam as measured with the gas jet and the residual gas.

The broadening of the image and resulting poorer signal quality caused by the thermal velocity of the residual gas particles as compared to the signal from the cold jet can be clearly observed. Also, a higher intensity from the jet as compared to the signal from the residual gas can be seen. Note that the lateral displacement between the two profiles is a direct result of the high jet velocity.

Image Resolution and Reaction Rate

The resolution of this monitor can be influenced by many factors such as the resolution of the camera and the MCP, image broadening caused by the gas jet screen thickness and homogeneity, thermal spread of the generated ions, space charge of the primary beam and the external field. For the specific setup at the Cockcroft Institute, the camera resolution is given by the size of one pixel which is σ_{CCD} = 90 μm. The MCP has two plates stacked in a chevron configuration, and its resolution is estimated as σ_{MCP} = 80 μm. The gas jet thickness only affects the resolution along one axis. Since the electron beam current is low, effects from space charge can be ignored. An ROI was used to analyze the measured profiles, as indicated by the black dashed line in Fig. 5. The fitting procedure yields beam sizes of

$\sigma_{x\_jet} = 0.54 \pm 0.02$ mm and $\sigma_{y\_jet} = 0.56 \pm 0.03$ mm for the gas jet , as well as $\sigma_{x\_res} = 1.34 \pm 0.02$ mm for the residual gas image. Similarly, the beam size in the X direction is $\sigma_{x\_real} = 0.53$ mm. For the Y-axis, considering the jet thickness of 0.28 mm and the thermal spread accordingly, the beam size is $\sigma_{y\_real} = 0.47$ mm. It should be pointed out that for every application, the skimmer size must be chosen carefully, based on both, the acquisition time and the overall resolution requirements.

The thermal spread process under the action of an external field was simulated in WARP [33] using the same voltage setting used for the measurement shown in Fig. 5. Initially, a round Gaussian N_2^+ beam was created at the interaction point assuming 10^6 particles. It was further assumed that the N_2^+ ions have the same velocity spread as the N_2 gas jet, the temperature of which is 10 K. The initial rms beam size was assumed to be 0.50 mm.

Fig. 6 below shows an example of a simulated result of an ion beam drifting towards the MCP with an initial beam size of 0.53x0.47 mm^2. It also shows a larger image broadening in the residual gas image than in the gas jet image. The rms size measured from the simulation data is $\sigma_{x\_jet} = 0.54$ mm, $\sigma_{y\_jet} = 0.60$ mm for the gas jet image and $\sigma_{x\_res} = 1.06$ mm for the residual gas image. The separation of both images along the x direction is 2.62 mm.

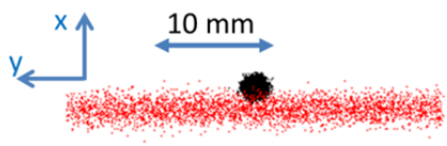

Figure 6: Simulated beam image at the location of the micro channel plate.

These results agree well with the experimentally observed values and indicate a good understanding of the various processes in the monitor.

The reaction rate R in the monitor is given by

$$R = P_{ion} \cdot I / q_p \quad (1)$$

where P_{ion} is the probability of ionization of a gas molecule by the projectile beam, I is the projectile flux in particles per second or projectile current, and q_p is the projectile charge. The probability can be expressed as

$$P_{ion} = \sigma_{ion} \cdot \rho_{gas} \cdot d_{gas} \quad (2)$$

where σ_{ion} is the ionization cross section, ρ_{gas} is the gas target number density and d_{gas} is the gas curtain thickness. These equations can be used to determine the required gas jet density for a specific primary beam to achieve a certain number of reactions per time.

Quantum Gas Jet

Due to the thickness of the gas jet, as well as space charge effects from an intense beam, it is unlikely that a monitor based on a curtain gas jet will achieve a sufficiently small resolution to measure sub-mm, although this might be a requirement for some applications. To overcome this issue, it was proposed to develop a gas jet scanner [34]. In this case, a thin pencil beam must be generated and is then moved through the beam to measure the profile. The device would be analogous to a wire scanner, but since it is minimally interceptive it can be scanned much more slowly. The beam intensity at each position could be derived by extracting and counting ions, as with the current setup. However, the trajectory of the ions would not be important, since the position information is provided by the gas jet position, so the profile measurement would not be affected by space charge. Alternatively, reliance on charged particles could be eliminated altogether by recording the beam losses during the gas jet scan or by detecting bremsstrahlung photons. To achieve a thin gas jet with a diameter below 100 µm, a novel focusing method is being developed for the generation of the gas jet. The quantum wavefunction of the neutral gas atoms is used to generate an interference pattern with a single maximum, which acts as an ultra-thin gas jet. A similar technique has been used successfully to create a neutral-Helium matter-wave microscope [35]. A Fresnel Zone Plate (FZP) was used to create a focal spot of 2 µm FWHM.

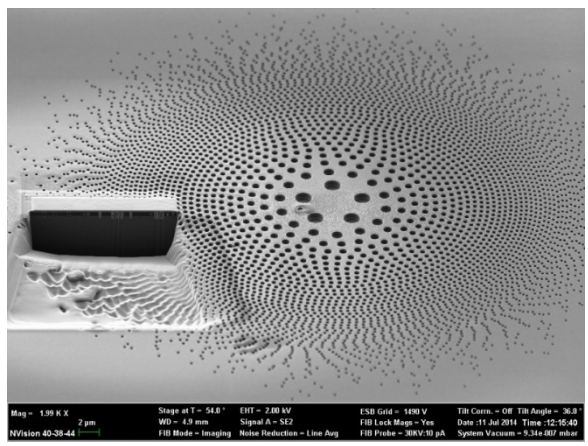

Figure 7: Focused Ion Beam image of the atomic sieve in production. The large hole on the left of the image has been cut into this test plate to check that the holes completely penetrate the silicon nitride film.

A Fresnel Zone Plate consists of a series of alternating open (transmitting) and closed (blocking) concentric rings. The width of the rings is chosen such that the path difference of a wave/particle passing through adjacent open rings to reach the focal point is equal to one wavelength. This is achieved if the open rings are centered at radii $r_n = (nf\lambda)^{(1/2)}$ where f is the focal length of the FZP and λ is the wavelength to be focused. Since only the

ISBN 978-3-95450-182-3

relative path length is important, *n* may begin at any number, so long as it is incremented by 2 for each successive open ring. The rings become narrower the further from the center they are, such that the area of each ring is the same. In addition, the resolution of the FZP is approximately equal to the width of the smallest (outermost) zone. Thus, it is desirable to have as many zones as possible, to maximize the transmitted power and produce a tight focus. However, for a small wavelength the zones must be extremely small in order to produce an acceptable focal length, so that manufacturing constraints limit the number of zones which can be produced. The focal length for a given FZP is inversely proportional to the wavelength. Thus, FZPs suffer from large chromatic aberration if the wave to be focused is not monochromatic. To use this particle-wave focusing, a conventional Helium jet will be generated using the current setup. However, the final skimmer will be replaced with the diffractive focusing plate. During the expansion of the jet from the orifice, the gas is adiabatically cooled. Almost all the thermal motion of the gas atoms is converted into forward motion of the gas jet, leaving a very small velocity spread. Thus, the jet can be considered to be almost monochromatic. It can be seen that in order to make the wavelength as large as possible, a light gas species should be chosen. For Helium at 300K, λ=0.08 nm. FZPs are used at similar wavelengths for x-ray focusing. However, x-ray FZPs are usually constructed from metal rings attached to an x-ray transparent substrate. In the case of the gas-focusing FZP, the open zones must allow gas atoms to pass, so no substrate can be used. For the matter-wave microscope, the plates were etched from a thin film of silicon nitride, and struts were added in order to support the inner zones [36].

In a collaboration between CERN and the Cockcroft Institute a focusing plate based on the photon sieve [37] is used. In the photon sieve, the concentric rings of the FZP are replaced with a series of small circular holes. Each hole is centered at the radius of an open zone in the equivalent FZP. It has been shown that a photon sieve with the same number of zones can create a sharper focus than the equivalent FZP. In addition, the sharp cut-off at the edge of the FZP causes higher-order diffraction which leads to side-lobes close to the focal spot. In a photon sieve, the intensity of side-lobes can be reduced if the fraction of each ring that is filled with holes is gradually reduced. The sieve is then said to be apodised [38]. Taking the above considerations into account, an 'atomic sieve' has been designed, applying the principle of the photon sieve to quantum matter-wave focusing. This atomic sieve consists of 5,230 holes, the smallest having a diameter of 80 nm and the largest 1.5 µm. The holes are etched into a 2 µm membrane of silicon nitride. Several plates have been successfully produced and first measurements at the university of Bergen have shown a jet diameter of only 30 mm. A focused ion beam image of one of the test plates is shown in Fig. 7.

CONCLUSION AND OUTLOOK

This paper has given an overview of least invasive beam monitors that rely on gas ionization or excitation. It summarized in particular some of the experimental results that have been obtained at the Cockcroft Institute to date.

The functioning principles of different gas-based monitors was first briefly explained and their individual limitations were discussed. This was followed by a more detailed analysis of the performance of the gas-jet based monitor, its resolution, and how pulsed mode operation can help avoid some of the problems encountered in DC operation.

Recently, a 3-dimensional translation stage has been installed in the setup, equipped with an ionization gauge, which will allow measuring the 3-dimensional gas jet density distribution and pave a way to a better understanding of gas dynamics overall. This will be essential to resolve systematic errors due to gas inhomogeneity and the resolution of the monitor. The ideas behind a novel quasi-optical focusing system based on Fresnel Zone Plates have also been presented. This should allow the generation of ultra-thin jets with a diameter of a few tens of microns. In experiments, a jet diameter of only 30 µm was already measured which marks a significant improvement compared to skimmer-shaped jets.

The gas jet monitor has great potential as a non-invasive beam profile measurement system, especially for high-intensity beams such as the CLIC Drive Beam and the European Spallation Source. For these applications, an extra magnetic field can be applied to reduce the distortion caused by space charge from the projectile beam. Further work is ongoing to evaluate the effect of the beam space charge in such situations.

On the basis of the monitor presented here, a fluorescence-based monitor is currently being developed in collaboration between the University of Liverpool/Cockcroft Institute, CERN and GSI as a key diagnostic for the HLLHC electron lens and the primary HLLHC proton beam itself. A second gas jet setup will be established at the Cockcroft Institute in 2017. A third prototype which will meet all HLLHC requirements will be based on the experiences gained in these studies and will be built in 2019.

ACKNOWLEDGEMENT

Many colleagues have contributed to this paper and the development of the respective monitors. The contributions of N.S. Chritin, E.B. Diaz, P. Forck, A. Jeff, O.R. Jones, K.U. Kühnel, E. Martin, M. Putignano, G. Schneider, V. Tzoganis, S. Udrea, R. Veness and H.D. Zhang (in alphabetic order), the MPI-K, CERN and Daresbury design offices and workshops are acknowledged.

REFERENCES

[1] M. Eshraqi, et al., The ESS Linac, *Proc. IPAC2014*, Dresden, Germany, 2014 pp.THPME043.

[2] C. P. Welsch, et al., Ultra-low energy storage ring at FLAIR, *Hyperfine Interact*., vol. 213, no. 1–3, pp. 205–215, 2012.

[3] V. Chohan (editor), "Extra Low Energy Antiproton ring (ELENA) and its Transfer Lines, Design Report," CERN-2014-002 (2014).

[4] T. Giacomini, et al., Ionization profile monitors - IPM @ GSI, *Proceedings of DIPAC2011*, Hamburg, Germany, pp. TUPD51, 2011.

[5] J. Mießner, et al., An ionization profile monitor for the determination of the FLASH photon beam parameter, *Nucl. Instruments Methods Phys. Res. Sect. A Accel. Spectrometers, Detect. Assoc. Equip.*, vol. 635, no. 1 SUPPL., pp. S104–S107, 2011.

[6] T. Tsang, et al., Residual gas fluorescence monitor for relativistic heavy ions at RHIC, *Phys. Rev. Spec. Top. - Accel. Beams*, vol. 16, no. 10, p. 102802, 2013.

[7] D.A. Bartkoski, et al., Design of an ionization profile monitor for the SNS accumulator ring, *Nucl. Instruments Methods Phys. Res. Sect. A Accel. Spectrometers, Detect. Assoc. Equip.*, vol. 767, pp. 379–384, 2014.

[8] R. Connolly, et al., Beam profile measurements and transverse phase-space reconstruction on the relativistic heavy-ion collider, *Nucl. Instruments Methods Phys. Res. Sect. A Accel. Spectrometers, Detect. Assoc. Equip.,* vol. 443, pp. 215-222, 2000.

[9] P. Forck, Minimal Invasive Beam Profile Monitors for High Intense Hadron Beams, *Proceedings of IPAC2010*, Kyoto, Japan, pp. TUZMH01, 2010.

[10] F. Becker et al., Beam induced fluorescence (BIF) monitor for intense heavy ion beams, *Proceedings of BIW2008*, Tahoe City, California, USA, pp. TUPTPF054, 2008.

[11] F. Becker et al., beam induced fluorescence - profile monitoring for targets and transport, *Proceedings of HB2012*, Beijing, China, pp. THO3C03, 2012.

[12] M. Putignano, et al., A fast, low perturbation ionization beam profile monitor based on a gas-jet curtain for the ultra-low energy storage ring, *Hyperfine Interact.*, vol. 194, no. 1–3, pp. 189–193, Aug. 2009.

[13] B. Vosicki and K. Zankel, The sodium curtain beam profile monitor of the ISR, *IEEE Transactions on Nuclear Science*, vol. 22, no.3, pp. 1475–1478,1975.

[14] A. Bubley, et al., Magnesium jet profile monitor, *Proceedings of 17th International Conference on High Energy Accelerators*, Dubna, Russia, pp. 357-359, 1998.

[15] R. Galiana, et al., A carbon jet beam profile monitor for LEAR. *Proceedings of PAC91*, San Francisco, CA, USA, pp. 1198–1200, 1991.

[16] E. Takada, Carbon ion radiotherapy at NIRS-HIMAC, *Nucl. Phys. A*, vol. 834, no. 1-4, pp. 730c–735c, 2010.

[17] Y. Hashimoto, et al., Oxygen gas-sheet beam profile monitor for the synchrotron and storage ring, *Nucl. Instr. Meth. A*, vol. 527, no. 3, pp. 289–300, 2004.

[18] T. Fujisawa, et al., Multi-pole magnets to focus an O_2 sheet beam for a non-destructive beam-profile monitor, *Nucl. Instr. Meth. A*, vol. 506, no. 1-2, pp. 50–59, 2003.

[19] S. Sawada, J-PARC Facility, *Nucl. Phys. A*, vol. 834, no. 1–4, p. 701c–706c, 2010.

[20] Y. Hashimoto, et al., Development of a beam profile monitor using nitrogen molecular jet for intense beams, *Proc. IBIC2012*, Tsukuba, Japan, pp. TUPB73, 2012.

[21] Y. Hashimoto, et al., Development of a beam profile monitor using a nitrogen-molecular jet for the J-PARC MR, *Proc. IBIC2013*, Oxford, UK, pp. WEPF17, 2013.

[22] T. Tsang et al., Optical beam profile monitor and residual gas fluorescence at the relativistic heavy ion collider polarized hydrogen jet, *Review of Scientific Instruments* vol. 79, no. 10, pp. 105103, 2008

[23] J. Ullrich, et al., Recoil-ion and electron momentum spectroscopy: reaction-microscopes, *Rep. Prog. Phys.*, vol. 66, no. 9, pp. 1463–1545, 2003.

[24] M. Putignano, Supersonic gas-jet based beam profile monitor, *PhD thesis*, University of Liverpool, 2012.

[25] V. Tzoganis, et al., Design and first operation of a supersonic gas jet based beam profile monitor at the Cockcroft Institute, *Phys. Rev. AB*, accepted (2017).

[26] G. Scoles, et al. (ed.), Atomic and Molecular Beam Methods Vol. 1, Oxford Univ. Press, 1988.

[27] MHE3-MS1H-3/2G-1/8 solenoid pulsed valve by Festo, `www.festo.com/cat/no_no/products_MH2`

[28] TGP110 pulse generator by Aim & Thurlby Thandar Instruments, `www.aimtti.com`

[29] DC power supply IPS-3303 by ISO-Tech, `www.iso-techonline.com`

[30] Solid state relay DMO063 by Crydom, `www.crydom.com/en`

[31] V. Tzoganis and C. P. Welsch, A non-invasive beam profile monitor for charged particle beams, *Appl. Phys. Lett.*, vol. 104, no. 20, 2014.

[32] V. Tzoganis, et al., Gas dynamics considerations in a non-invasive profile monitor for charged particle beams, *Vacuum*, vol. 109, pp. 417–424, 2014.

[33] A. Friedman, et al., *IEEE Trans. Plasma Sci.,* vol. 42, no. 5, pp. 1321–1334, 2014.

[34] A. Jeff, et al., Quantum Gas Jet for Non-Invasive Beam Profile Measurement, *Proc. IBIC2014*, Monterey, CA, USA, TUCZB3, 2014.

[35] M. Koch, S. Rehbein, G. Schmahl, T. Reisinger, G. Bracco, W.E. Ernst, et al., "Imaging with neutral atoms: a new matter-wave microscope", *J. Microsc.,* 229 (2008).

[36] T. Reisinger, S. Eder, M.M. Greve, H.I. Smith, B. Holst, "Free-standing silicon-nitride zoneplates for neutral-helium microscopy", *Microelectron. Eng.* 87 (2010) p1011–1014.

[37] L. Kipp, M. Skibowski, R. Johnson, R. Berndt, "Sharper images by focusing soft X-rays with photon sieves", Nature 414 (2001).

[38] A. Sabatyan, P. Roshaninejad, "Super-resolving random-Gaussian apodized photon sieve", *Appl. Opt.* 51 (2012) p6315–6318.

ISBN 978-3-95450-182-3